RSC Advances

RSC Publishing

PAPER

Improved electrocatalytic stability in ethanol oxidation by microwave-assisted selective deposition of SnO_2 and Pt onto carbon

Cite this: *RSC Advances*, 2013, **3**, 7001

Patrícia A. Russo,†[a] Minjeh Ahn,†[b] Yung-Eun Sung*[c] and Nicola Pinna*[abd]

Received 25th January 2013,
Accepted 28th February 2013

DOI: 10.1039/c3ra40427g

www.rsc.org/advances

$Pt/SnO_2/C$ nanostructures with SnO_2/Pt molar ratios ranging from 2.5 to 0.6 were synthesized by simple and fast microwave assisted routes. The materials are composed of 3 5 nm SnO_2 and Pt nanoparticles dispersed on the carbon support, with the morphology of the coating depending on the SnO_2/Pt ratio: a homogenous layer of nanoparticles coating the carbon surface is obtained for SnO_2/Pt of 2.5, whereas small Pt SnO_2 clusters are formed for lower ratios. The electrocatalytic activity of the composites on the ethanol oxidation reaction (EOR) was studied by cyclic voltammetry and chronoamperometry. All the binary catalysts exhibited lower onset potentials for the EOR and slower decay of the current density with time than a commercial Pt/C catalyst. However, improved peak current densities were only observed for the composites with ratios 1.6, 1.0 and 0.6, indicating that the formation of metal and metal oxide nanoparticles clusters is favorable for the EOR. This morphology facilitates the hydroxyl groups transfer from the metal oxide to the platinum at low potentials and also the electron transfer between carbon and platinum. The best overall performance was found for the catalyst with $SnO_2/Pt = 1$, on which the number of three phase boundaries is maximized. Moreover, the catalyst with $SnO_2/Pt = 1$ continued to exhibit significantly better catalytic performance on the EOR than the commercial catalyst after potential cycling.

Introduction

Polymer electrolyte membrane fuel cells (PEMFCs) are environmental friendly electrochemical conversion devices promising for transportation and small portable electronic applications. Ethanol is a especially attractive fuel for PEMFCs due to its high theoretical volumetric energy density (8 kWh Kg^{-1}), easy storage and transportation, low toxicity (compared to methanol for instance) and easy production from biomass and agricultural products such as sugar cane.[1–3]

Platinum is one of the most active catalysts for the ethanol oxidation reaction (EOR). However, the oxidation of ethanol to CO_2 is a difficult and complex process that requires breaking of C–C bonds and may involve several different mechanism pathways with the formation of a high number of reaction intermediates such as CO, CH_x species or acetaldehyde.[1,3–5] These intermediate species strongly adsorb on the platinum surface, poisoning the catalyst by occupying the active sites, which leads consequently to a decrease of the catalytic activity.[4,6] The use of metal oxides such as RuO_2, CeO_2, TiO_2, ZrO_2, ATO or SnO_2 either as platinum support or co-support, has been proposed in order to improve the performance of Pt-based catalysts in the oxidation of ethanol.[7–19] In particular, the ability of tin dioxide to promote the oxidation of intermediate CO by providing oxygen species according to the bi-functional mechanism is well known.[2,6,11,14] In fact, materials containing SnO_2 in their composition have shown promising electrocatalytic activities on the EOR.[2,3,15,20] For example, high peak current densities have been reported for the ethanol electrooxidation catalyzed by SnO_2@Pt/C core–shell structures.[2] The authors suggested that a change of the Pt electronic structure induced by the particular Pt–SnO_2 structure could be responsible for the activity enhancement observed.

Benzyl alcohol has proven to be a suitable medium for the synthesis of a high variety of metal oxide nanoparticles[21–24] and hybrid materials.[25] Non-aqueous sol–gel routes to metal oxide nanoparticles have several advantages compared for example with the more traditional aqueous sol–gel, including a better control over the size and morphology of the particles, due to the lower reactivity of the metal oxide precursors in non-hydrolytic media, and higher crystallinity of the products.

[a]*Department of Chemistry, CICECO, University of Aveiro, 3810 193, Aveiro, Portugal*
[b]*World Class University (WCU) program of Chemical Convergence for Energy & Environment (C2E2), School of Chemical and Biological Engineering, College of Engineering, Seoul National University (SNU), Seoul, 151 744, Korea.*
E mail: nicola.pinna@hu berlin.de
[c]*Center for Nanoparticle Research, Institute for Basic Science, and School of Chemical and Biological Engineering, Seoul National University, Seoul 151 742, Korea. E mail: ysung@snu.ac.kr*
[d]*Humboldt Universitat zu Berlin, Institut fur Chemie, Brook Taylor Straße 2, 12489, Berlin*
† These authors equally participated to the work

In the particular case of the ''benzyl alcohol route'', the solvent acts as oxygen donor for the synthesis of the metal oxide and as ligand, allowing the control over the nanoparticle size without the need of additional stabilizing agents. This offers further advantages over other non-hydrolytic routes, namely the high purity of the fabricated materials.[26] The use of microwave heating for the synthesis of nanomaterials is becoming increasingly popular, as it considerably decreases the reaction times and improves yields and reproducibility. Microwave heating also brings great advantages to the synthesis of nanoparticles in benzyl alcohol, allowing the preparation of metal oxides in a few minutes.[27–29] Moreover, our group has recently reported the one-pot microwave-assisted synthesis of metal oxides/reduced graphene oxide (RGO) nanocomposites in benzyl alcohol.[30] Tin oxide/RGO and magnetite/RGO composites were produced in 5–10 min and a more homogeneous coating of the RGO sheets was attained when microwave heating was applied instead of the traditional heating methods. Here, we use this approach to prepare binary Pt–SnO_2 electroctalysts supported on carbon black, for the oxidation of ethanol in acidic medium at room temperature. Pt/SnO_2/C composites with different SnO_2/Pt ratios and coating morphologies were produced in this manner. The activity of the catalysts on the EOR was studied by cyclic voltammetry and chronoamperometry and their electrochemical stability was assessed by potential cycling.

Experimental

Synthesis of the composites

Carbon black Vulcan XC72 was used as support of the tin oxide and platinum nanoparticles. The carbon (1 g) was previously oxidized by refluxing in 5 M HNO_3 at 80 °C for 4 h, washed with water and dried. Deposition of the SnO_2 and Pt nanoparticles was performed by microwave-assisted synthesis routes previously reported.[30,31] First, SnO_2/C composites with amounts of tin oxide ranging from 10 to 50 wt% were prepared by changing the quantities of carbon support and metal oxide precursor used in the synthesis. Briefly, suitable quantities of carbon and tin(IV) chloride (99.995%, Aldrich) were placed in a microwave vial containing 20 mL of benzyl alcohol, under argon. The mixture was sonicated to disperse the carbon material and then heated in a CEM Discover SP microwave at 185 °C for 10 min. The solid was collected by centrifugation, washed with tetrahydrofuran and dried at 65 °C. Platinum NPs were then deposited onto the SnO_2/C materials by a microwave-assisted ''polyol'' method. In all cases the amount of Pt deposited was 20 wt%: 0.10 g of the SnO_2/C nanocomposite was added to a solution of 0.053 g of H_2PtCl_6 (99.995%, Aldrich) in 20 mL of ethylene glycol, under argon. A solution of NaOH in ethylene glycol was added to raise the pH to 11–12. The suspension was sonicated for 10 min and submitted to microwave irradiation for 5 min at 140 °C. The final solid was recovered by centrifugation, washed with ethanol and ultrapure water and dried at 65 °C.

Characterization

The X-ray powder diffraction patterns were recorded on a PANalytical X'Pert MPD diffractometer at 45 kV and 40 mA, using Cu-Kα radiation (λ = 0.1541 nm). The carbon content of the samples was determined with a TruSpec 630 elemental analyzer. Nitrogen adsorption isotherms at 196 °C were measured on a Micromeritics Gemini. Prior to the measurements the samples were outgassed at 150 °C overnight. The micropore volume and external surface area of the uncoated carbon were calculated by the α_s method using standard data for nitrogen adsorption on non porous carbon.[32] Scanning electron microscopy (SEM) images were recorded with a Hitachi SU-70 microscope operating at 15 kV. Transmission electron microscopy (TEM) and high resolution TEM (HRTEM) images were obtained on a Hitachi H9000 at an accelerating voltage of 300 kV, and a Philips CM200 FEG operated at an accelerating voltage of 200 kV. Energy dispersive X-ray spectroscopy (EDS) analysis was performed with a Bruker Quantax 400. The error associated with the determination of the platinum and tin atomic percentages by EDS was below 20% for all the samples investigated (ICP-AES analysis was performed for some of the samples and the corresponding SnO_2/Pt ratios were found to be in agreement with the EDS results). High-resolution X-ray photoelectron spectroscopy (HR-XPS) measurements were performed on the soft X-ray beam line (8A1) connected to an undulator (U7) at the Pohang Accelerator Laboratory (PAL). The end station was composed of a high performance electron analyzer (SCIENTA-200) with energy and angular resolution of 5 meV and 0.5°, respectively. The experiment was carried out in an ultrahigh vacuum (UHV) chamber with a base pressure $\leqslant 5 \times 10^{-10}$ Torr. All spectra were measured using 630 eV of incident photon energy.

Electrochemical experiments

The electrochemical measurements were performed in a three-electrode electrochemical cell using a glassy carbon electrode as a working electrode, platinum wire as a counter-electrode and a saturated calomel electrode (SCE) as a reference electrode. All electrochemical data were recorded against the reversible hydrogen electrode (RHE). Catalyst inks were prepared by mixing 0.01 g of the composite material with 50 μL of DI water, 600 μL of 2-propanol and 15 μL of a 5 wt% Nafion solution (Aldrich), after which it was dropped onto the glassy carbon electrode with a micropipette and dried. The activity of the materials for the ethanol oxidation reaction (EOR) was studied by cyclic voltammetry conducted at room temperature and at a scan rate of 20 mV s^{-1}, in an oxygen-free solution of 0.1 M $HClO_4$ and 0.1 M ethanol purged with argon. The chronoamperometric measurements were performed in a 0.1 M $HClO_4$ and 0.1 M ethanol solution at a constant potential of 0.5 V for 1000 s. In order to assess the electrochemical stability, accelerated degradation tests (ADT) were performed: the composites were submitted to 1000 potential cycles in 0.1 M $HClO_4$ at a scan rate of 100 mV s^{-1}. For comparison, the activity of commercial Pt/C catalyst (Johnson Matthey) with 20 wt% Pt on the EOR was also tested in the same conditions.

Table 1 Quantities of metal oxide precursor and carbon used in the synthesis, and composition and textural characteristics of the prepared $Pt/SnO_2/C$ catalysts

Sample	Carbon/g	Metal oxide precursor/mmol	C wt%[a]	SnO_2/Pt[b]	$S_{BET}/m^2\ g^{-1}$	$V_{p(0.95)}/cm^3\ g^{-1}$[c]
$Pt/SnO_2/C$ 1	0.30	2.00	42	2.5	108	0.16
$Pt/SnO_2/C$ 2	0.40	1.14	56	1.6	134	0.18
$Pt/SnO_2/C$ 3	0.48	0.80	66	1.0	154	0.24
$Pt/SnO_2/C$ 4	0.52	0.39	69	0.6	142	0.24

[a] Carbon weight percentage determined by CHNS elemental analysis. [b] Molar SnO_2/Pt ratio estimated by EDS. [c] Pore volume obtained at p/p^0 0.95.

Results and discussion

Catalysts characterization

To prepare the $Pt/SnO_2/C$ nanocomposites, several amounts of tin dioxide were first deposited on the surface of the carbon black particles, by reaction of tin(IV) chloride in benzyl alcohol in the presence of the carbon and under microwave irradiation. This approach was recently reported by our group to prepare tin dioxide/reduced graphene oxide nanocomposites in short times and with high yields.[30] It has been extended here for the coating of a common carbon support used in electrocatalysis (Carbon black Vulcan XC72) in order to produce catalysts for ethanol electrooxidation. Identical amounts of platinum (20 wt%) were then deposited on all the SnO_2/C composites.

The quantity of metal oxide precursor and carbon black used in the synthesis, and the chemical composition and textural characteristics of the obtained materials are registered in Table 1. The carbon content and SnO_2/Pt molar ratio of the composites were determined by carbon elemental analysis and EDS (Fig. 1b), respectively, and the results obtained are in close agreement with the nominal values. Since the platinum wt% is the same in all samples, the decrease of the SnO_2/Pt ratio reflects the decrease of the metal oxide content of the materials. The proximity between the nominal and experimental chemical composition of the fabricated materials, reflects another advantage of the microwave heating: owing to the higher microwave absorption ability of the carbon particles compared to the solvent, the nanoparticles selectively grow on the carbon surface, in a process promoted by the surface functional groups. Therefore, the formation of free or weakly attached particles is minimized, which leads to a more precise control over the composition of the materials and higher reproducibility. Table 1 also shows the apparent BET surface areas and pore volumes of the samples. The uncoated carbon support, *i.e.*, the oxidized carbon black, has S_{BET} of 253 $m^2\ g^{-1}$, micropore volume of 0.045 $cm^3\ g^{-1}$ and surface area external to the micropores of 146 $m^2\ g^{-1}$. The deposition of tin oxide and platinum NPs on the carbon surface leads to a considerable decrease of the surface area and pore volume, probably caused by partial or complete blockage of the microporosity of the support. As expected, in general the surface area and pore volume decreases as the amount of tin oxide deposited on the carbon surface increases, with the samples containing the lowest amounts of metal oxide NPs having similar textural characteristics.

Fig. 2 shows the X-ray diffraction patterns of the composites with different SnO_2/Pt ratios. All diffractograms exhibit peaks of the cassiterite structure of SnO_2 (JCPDS file no. 41-1445) and of the face-centered cubic platinum lattice (JCPDS file no. 87-0640). Specifically, diffraction by the (111), (200) and (220) lattice planes of platinum are observed at approximately 39, 46 and 67° (2θ), while the diffraction peaks associated with the (110), (101) and (211) planes of the tin oxide structure are seen at approximately 26, 34 and 52° (2θ). The change in the SnO_2/Pt ratio of the samples is noticeable on the variation of the intensity of the corresponding reflections: as the amount of tin oxide nanoparticles decreases, the corresponding diffraction peaks become progressively less intense. The average size of

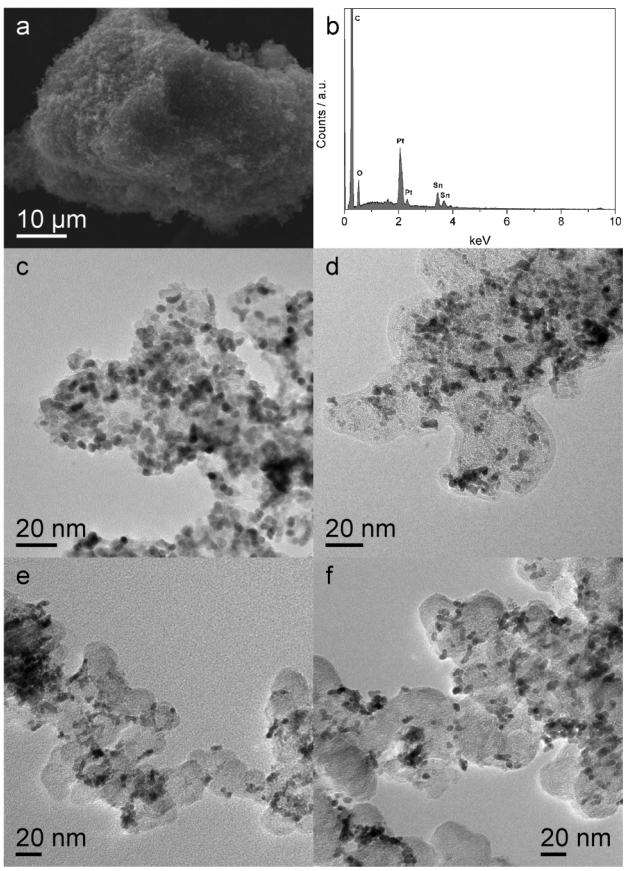

Fig. 1 SEM image of $Pt/SnO_2/C$ 3 (a) and EDS spectrum (b); TEM images of the $Pt/SnO_2/C$ 1 (c), $Pt/SnO_2/C$ 2 (d), $Pt/SnO_2/C$ 3 (e) and $Pt/SnO_2/C$ 4 (f) composites.

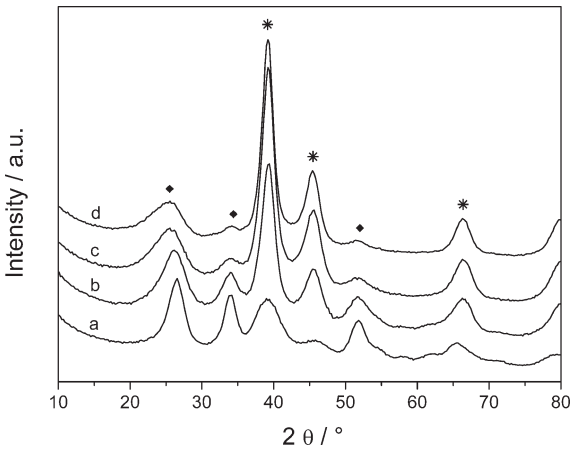

Fig. 2 X ray powder diffraction patterns of Pt/SnO_2/C 1 (a), Pt/SnO_2/C 2 (b), Pt/SnO_2/C 3 (c) and Pt/SnO_2/C 4 (d) nanocomposites (◆ and * indicate the most intense reflections of the SnO_2 and Pt structures, respectively).

the tin oxide nanoparticles, estimated with the Scherrer equation from the XRD data of the Pt/SnO_2/C composites and SnO_2/C samples prior to Pt deposition, is *ca.* 5, 4, 4 and 4 nm for SnO_2/Pt ratios of 2.5, 1.6, 1.0 and 0.6, respectively. The slight decrease of the average particle size with the decrease of the SnO_2/Pt ratio can be attributed to the decrease of the amount of metal oxide precursor added to the synthesis in order to produce composites with low tin oxide weight%. On the other hand, the average size of the Pt nanoparticles estimated from the (200) reflection is *ca.* 3, 4, 4 and 4 nm for SnO_2/Pt ratios of 2.5, 1.6, 1.0 and 0.6, respectively. The calculated average size of the Pt nanoparticles is slightly lower for the highest SnO_2/Pt ratio, which can be explained by differences in the dispersion of the platinum nanoparticles on surfaces with distinct metal oxide coverage (the dispersion is better on the carbon with the highest amount of SnO_2).

Fig. 3 shows the Pt 4f and Sn 3d XPS spectra of the Pt/SnO_2/C-1 sample. The binding energy of Pt $4f_{7/2}$ is 70.9 eV (Fig. 3a), corresponding to platinum in the zero-valent state.[6,8] The binding energy of the Sn $3d_{5/2}$ peak (487.6 eV) indicates the presence of tin oxide on the material (Fig. 3b). The value is shifted to higher binding energies with respect to the binding energy corresponding to the Sn^{4+} oxidation state (486.4 eV).[33] Shifts in the binding energies can be attributed to interactions between the various components of the sample (SnO_2, Pt), as reported by other authors.[6,8]

The TEM images of the as-prepared nanocomposites (Fig. 1c–f) clearly show an increase in the density of the particles deposited on the surface of the carbon support with the increase of the SnO_2/Pt ratio. Moreover, the nanoparticles homogeneously coat the entire surface of the carbon particles in sample Pt/SnO_2/C-1. However, there seems to be a tendency towards the formation of nanoparticles agglomerates as the SnO_2/Pt ratio decreases, which consequently results in portions of the carbon surface being left uncoated. A representative HRTEM image is presented in Fig. 4. It shows an edge of a carbon particle containing an agglomerate of metal oxide and metal nanoparticles. Fig. 4b displays the

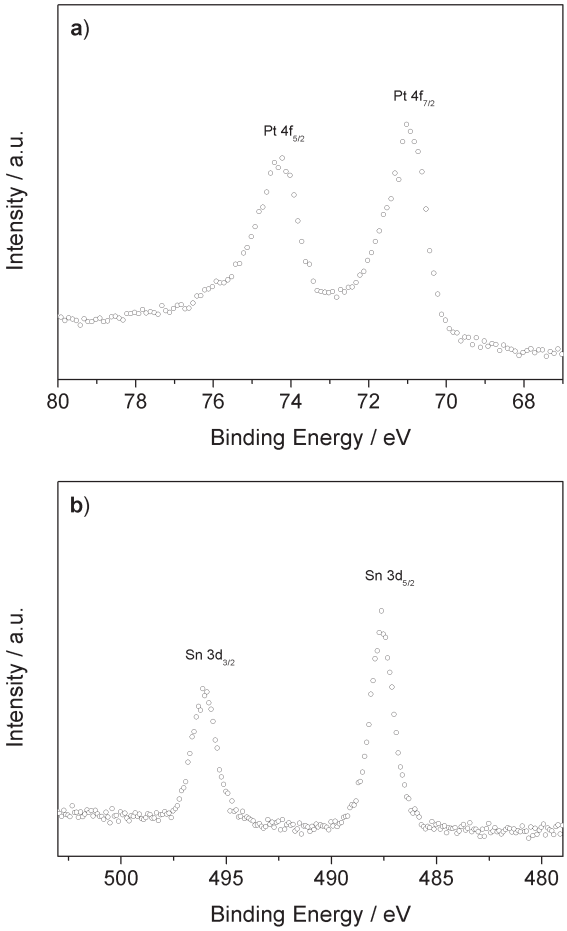

Fig. 3 Pt 4f (a) and Sn 3d (b) XPS spectra of Pt/SnO_2/C 1.

power spectrum (PS) of the whole image in Fig. 4a, showing reflections associated to the 111 and 200 lattice planes of platinum and 110 of the tin oxide cassiterite structure. Fig. 4 c

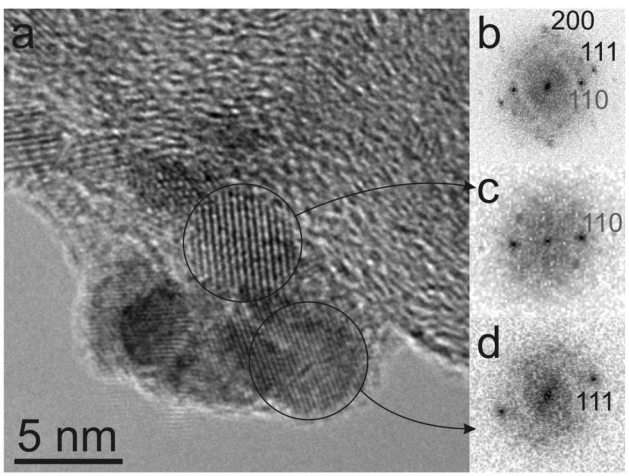

Fig. 4 High resolution TEM image of Pt/SnO_2/C 2 (a). Power spectra of the whole image (b) and of the delimited regions (c, d). Indices in grey for the SnO_2 cassiterite and in black for the Pt fcc structure, respectively.

and d are the PSs of the delimited regions in Fig. 4a and are due to SnO_2 and Pt nanoparticles, respectively. The particles are not oriented along a particular zone axis but the 3.35 Å and 2.27 Å reflections of the 110 and 111 lattice planes of the cassiterite and fcc Pt structures, respectively, are clearly visible. The size of the SnO_2 and Pt nanoparticles estimated from the TEM images is 3–5 nm in both cases, which is in close agreement with those calculated from the XRD data. From the study of many HRTEM images, it was found that the Pt nanoparticles preferentially nucleate, and are therefore deposited, at the SnO_2 sites. This is attributed to the fact that the platinum–metal oxide interactions are stronger than platinum–carbon interactions.[8,34] In the case of the materials with lower SnO_2/Pt ratios (Pt/SnO_2/C-2, Pt/SnO_2/C-3 and Pt/SnO_2/C-4), in which the quantity of tin dioxide is not enough to cover most of the carbon surface, as occurs with Pt/SnO_2/C-1, the higher affinity of the platinum for the metal oxide leads to the formation of small Pt–SnO_2 clusters, as shown in Fig. 4. As it will be shown below, this particular type of morphology is especially favorable for the ethanol oxidation reaction.

Electrocatalytic oxidation of ethanol

The electrochemical activity of the Pt/SnO_2/C nanocomposites toward the ethanol oxidation reaction was investigated by cyclic voltammetry and the results are presented in Fig. 5a. For comparison, the voltammogram of a commercial Pt/C catalyst with 20 wt% Pt is also presented. The curves show multiple oxidation peaks, similarly to results reported in the literature.[2,14,35] The multiple oxidation peaks are caused by intermediate species formed after the ethanol oxidation reaction, especially unstable carbon species that react rapidly on metal surfaces. Intermediate species that may be produced during ethanol oxidation include acetaldehyde, acetate or acetic acid, in addition to CH_x fragments.[1,3,36] The presence of many unstable intermediates during the electrochemical reactions also induces current perturbations during potential cycling, which can be minimized by controlling the scan rate, but not fully eradicated. The onset potential for the ethanol oxidation reaction is similar for all Pt/SnO_2/C catalysts (0.21 V), and 0.2 V lower than that of the Pt/C. This means that tin oxide decreases the activation energy of the reaction, so the oxidation starts at lower potential. Moreover, the onset potential is not influenced by the quantity of SnO_2 present on the sample. Additionally, the current density of the binary systems at low potential (0.4 V) is in all cases higher than that of Pt/C (between 2.5 and 4.6 times higher), with the lowest increase corresponding to the material with higher amount of metal oxide NPs and the maximum being observed for Pt/SnO_2/C-3. With the exception of Pt/SnO_2/C-1, the composites also produce higher peak currents densities than Pt/C (Fig. 5a and c). In particular, the anodic peak current density of ethanol oxidation on Pt/SnO_2/C-3 is approximately 33% higher than that of Pt/C. Therefore, all three catalysts with lower amounts of tin oxide show better performance for the electrocatalyic oxidation of ethanol at room temperature than the commercial catalyst, with the optimal performance being achieved with a SnO_2/Pt ratio of 1. It is worth noticing that improvement of the electrocatalytic activity of platinum by tin oxide has been reported by several other authors.[2,3,14,15,20] The

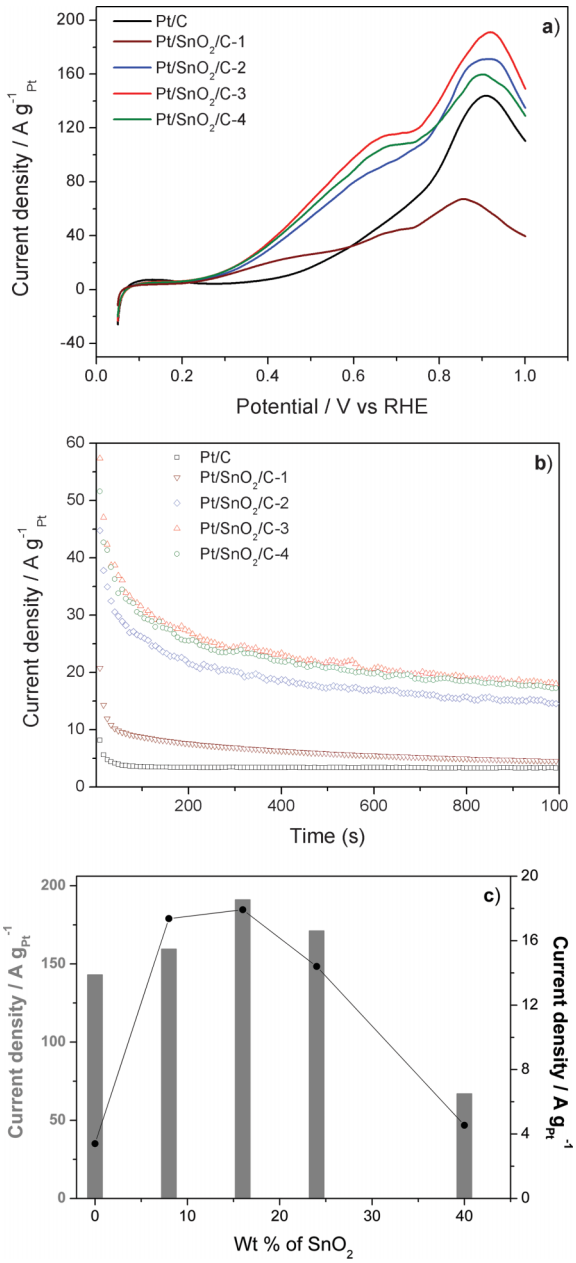

Fig. 5 a) Forward scans of the cyclic voltammograms of the Pt/SnO_2/C materials and Pt/C measured at room temperature in 0.1 M $HClO_4$/0.1 M ethanol solution with a scan rate of 20 mV s^{-1}; b) chronoamperometry curves of the Pt/SnO_2/C materials and Pt/C measured at room temperature and 0.5 V in 0.1 M $HClO_4$/0.1 M ethanol solution; c) forward peak current densities (bars) and current at 0.5 V after 1000 s (circles) as a function of the amount of tin dioxide in the Pt/SnO_2/C materials.

advantage of the materials described here is the simplicity and quickness of the procedure by which they are synthesized. Moreover, the characteristics of microwave heating lead to a selective growth of the nanoparticles on the carbon surface, therefore allowing a relatively precise control over the materials' composition.

The electrochemical active surface area (ECSA) is an important parameter affecting the performance of the cata-

lysts. However, the determination of ECSA by hydrogen desorption for materials containing metal oxides does not lead to highly exact values due to the presence of a high amount of functional groups on the metal oxide. Nevertheless, considering that (i) the size of the platinum nanoparticles is similar in the materials with SnO_2/Pt ratio of 1.6, 1.0 and 0.6; (ii) the amount of platinum is the same in all the samples; and (iii) the platinum was reduced after tin dioxide deposition, the ECSA of the samples should be similar, as reported by other authors.[19]

As mentioned before, the oxidation of ethanol at platinum surfaces involves a complex set of reactions and the formation of a high number of intermediate products, including CH_x, CH_xO or CO species, which can be further oxidized to CO_2.[1,4,15] Intermediate species such as CO adsorb strongly on the surface of the Pt catalyst, poisoning it by making the active sites unavailable for further reaction. The effect of tin oxide on the electrocatalytic activity of Pt has been extensively studied and is attributed to an increase of the CO-tolerance of the metal catalyst by the metal oxide (*i.e.*, to an anti-poisoning effect of the metal oxide), through a bi-functional mechanism[11,37] or an electronic effect,[2,15] which can also occur simultaneously. On the one hand, it has been reported that the metal oxide in contact with metal particles can change the electronic structure of the metal catalyst. These changes in the electronic structure can lead to a more efficient oxidation of the intermediates or to weaker Pt–CO interactions with a similar outcome.[2,15,38] On the other hand, the increase of the CO-tolerance of Pt through the bi-functional mechanism arises from the ability of tin oxide to dissociate water molecules at lower potentials than platinum, forming $(OH)_{ad}$ species that provide the oxygen required for the oxidation of CO to CO_2 at the metal surface and freeing the active sites.[11,37] Furthermore, it has also been suggested that saturation of SnO_2 sites by H_2O/OH weakens the interaction of water with Pt, making the metal active sites available for ethanol oxidation.[3] The decrease of the onset potential observed for all binary catalysts studied here and the peak current densities observed for some of them can be partially explained by these effects. However, the electrocatalytic performance of the composites clearly also depends on the morphology and quantity of the metal oxide nanoparticles present on the sample. When the carbon surface is homogeneously and almost entirely coated with tin dioxide and platinum nanoparticles, low oxidation peak current densities are observed (Pt/SnO_2/C-1). SnO_2 has low electrical conductivity, therefore, a high density of tin oxide nanoparticles dispersed on the carbon surface generates an isolating barrier that hinders the electron transfer between platinum and support. The electrocatalytic performance is significantly improved when small clusters of Pt and SnO_2 nanoparticles are formed. This morphology facilitates the hydroxyl groups transfer from the metal oxide to the platinum at low potentials and also the electron transfer between carbon and platinum. The optimal performance is obtained for a SnO_2/Pt ratio of 1.0, suggesting that the size and amount of the clusters also play an important role on the electrocatalytic activity, with the number of three-phase boundaries being maximized in this case. The number of interfacial regions between tin dioxide and platinum decreases for lower SnO_2/Pt ratios, *i.e.*, not all Pt nanoparticles are in contact with the metal oxide, which limits the OH transfer between metal oxide and metal.

Chronoamperometric measurements performed at 0.5 V for 1000 s are shown in Fig. 5c and are consistent with the CV data reported in Fig. 5a. The current densities of all the binary composite catalysts are higher than that of Pt/C during the measurement time. The decay of the current density with time during ethanol oxidation on Pt-based catalysts is attributed to the poisoning of the metal active sites by reaction intermediates like CO. The slower decrease of the current density observed for the Pt/SnO_2/C materials compared to the Pt/C catalyst reflects the promoting effect of tin oxide on CO oxidation (*i.e.*, its anti-poisoning effect) and the consequent higher electrochemical stability and efficiency of the former catalysts.

The electrochemical stability of the Pt/SnO_2/C-3 binary catalyst was further investigated by performing ADT (accelerated degradation test), which consisted of potential cycling between 0.5 and 1.0 V in 0.1 M $HClO_4$ at a scan rate of 100 mV s^{-1}. The CV and chronoamperometry curves of the Pt/SnO_2/C-3 catalyst before and after 1000 potential cycles are compared in

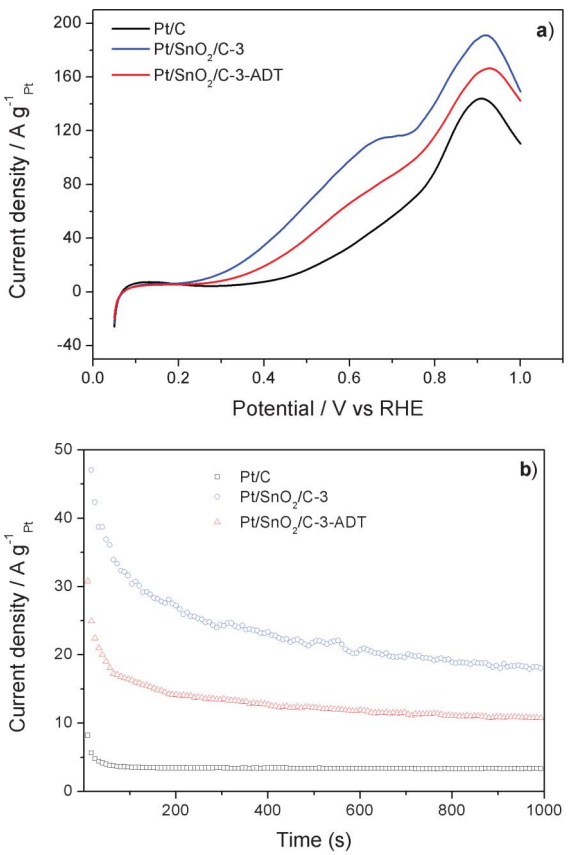

Fig. 6 a) Forward scans of the cyclic voltammograms of the Pt/SnO_2/C 3 catalyst before and after ADT and of Pt/C measured at room temperature in 0.1 M $HClO_4$/0.1 M ethanol solution with a scan rate of 20 mV s^{-1}; b) chronoamperometry curves of the Pt/SnO_2/C 3 catalyst before and after ADT and of Pt/C measured at room temperature and 0.5 V in 0.1 M $HClO_4$/0.1 M ethanol solution.

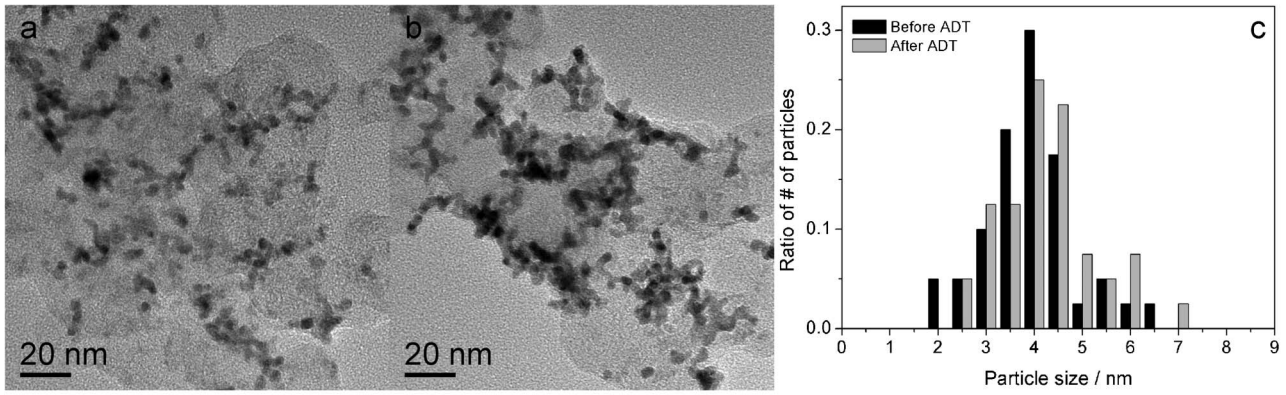

Fig. 7 TEM images of the Pt/SnO_2/C 3 catalyst (a) before and (b) after ADT; (c) particle size distribution before and after ADT obtained by analysis of TEM data of the samples.

Fig. 6 with the initial curves of Pt/C. TEM images of the material before and after ADT are also shown in Fig. 7. After potential cycling, a slight increase in the onset potential of ethanol oxidation (from 0.21 to 0.24 V) is observed, in addition to a decrease of the peak current density (*ca.* 13% for the anodic oxidation peak). Moreover, a faster decay of the current density with time is also seen (Fig. 6b). Nevertheless, even after 1000 cycles, the performance of the Pt/SnO_2/C-3 catalyst on the EOR is quite superior to that of the commercial one (Pt/C), indicating a significant stability of the former.

Continuous potential cycling in acidic media can lead to the growth and agglomeration of the platinum nanoparticles, either by redeposition of previously dissolved platinum or migration on the support surface. These processes, in turn, cause ECSA loss and consequently decrease the catalyst activity. As can be seen in Fig. 7, no drastic physical changes of the material are observed from the TEM images taken after ADT, in agreement with the catalytic results. Moreover, platinum particle size distributions before and after ADT (Fig. 7c), calculated by analysis of the TEM data, confirm this observation. A median particle size of 4.2 nm was found after ADT, against 3.9 nm obtained for the pristine material, which may account for the loss of performance observed. It has been shown before that metal oxides can have a stabilizing effect over platinum nanoparticles, because the interactions of the metal with the metal oxide are stronger than with the carbon surface,[8,34] which leads to lower rates of migration, agglomeration and growth of the metal particles during potential cycling.

Conclusions

SnO_2/C composites with several amounts of tin oxide nanoparticles were prepared by a simple and fast microwave-assisted synthesis in benzyl alcohol. Pt NPs were subsequently deposited by microwave-assisted ''polyol'' method. The morphology of the coating was found to depend on the amount of tin dioxide present on the material: a homogeneous coating of the carbon surface by a layer of nanoparticles was obtained for SnO_2/Pt of 2.5, while for lower ratios the nanoparticles tend to form agglomerates leaving high portion of the carbon surface uncoated. Moreover, the Pt nanoparticles preferentially nucleate at the SnO_2 sites and so they are deposited in their close contact, which results in the formation of small Pt–SnO_2 clusters on the materials with lower SnO_2/Pt ratios. The latter type of morphology was found to be more favorable for the electrocatalytic oxidation of ethanol. All the materials showed enhanced performance at low potential on the oxidation of ethanol at room temperature compared to a commercial Pt/C catalyst. However, the peak current densities were found to depend on the amount and morphology of the nanoparticles coating. Materials consisting of small Pt–SnO_2 clusters showed improved overall performances, with optimal results being obtained for SnO_2/Pt = 1. This morphology facilitates the hydroxyl groups transfer from the metal oxide to the platinum at low potentials and also the electron transfer between carbon and platinum, with the number of three-phase boundaries being maximized when SnO_2/Pt = 1. Furthermore, this composite continued to show significantly better catalytic activity on the EOR after 1000 potential cycles compared with the commercial catalyst.

Acknowledgements

This work was financially supported by the WCU (World Class University) program through the National Research Foundation (NRF) of Korea funded by the Ministry of Education, Science and Technology (R31-10013) and Fundação para a Ciência e a Tecnologia (FCT) project PTDC/CTM/098361/2008 and grant SFRH/BPD/79910/2011. Dr M.-G. Willinger and Prof. R. Schölgl from the Fritz Haber Institute of the Max Planck Society are acknowledged for the use of the CM200 FEG electron microscope and Catherine Marichy from the University of Aveiro for the measurements. YES acknowledges the support by the Research Center Program of IBS (Institute for Basic Science) in Korea.

References

1 A. Rabis, P. Rodriguez and T. J. Schmidt, *ACS Catal.*, 2012, **2**, 864.
2 J. C. M. Silva, R. F. B. De Souza, L. S. Parreira, E. T. Neto, M. L. Calegaro and M. C. Santos, *Appl. Catal., B*, 2010, **99**, 265.
3 A. Kowal, M. Li, M. Shao, K. Sasaki, M. B. Vukmirovic, J. Zhang, N. S. Marinkovic, P. Liu, A. I. Frenkel and R. R. Adzic, *Nat. Mater.*, 2009, **8**, 325.
4 S. C. S. Lai, S. E. F. Kleyn, V. Rosca and M. T. M. Koper, *J. Phys. Chem. C*, 2008, **112**, 19080.
5 J. M. Léger, S. Rousseau, C. Coutanceau, F. Hahn and C. Lamy, *Electrochim. Acta*, 2005, **50**, 5118.
6 X. Zhang, H. Zhu, Z. Guo, Y. Wei and F. Wang, *Int. J. Hydrogen Energy*, 2010, **35**, 8841.
7 H. Song, X. Qiu and F. Li, *Appl. Catal., A*, 2009, **364**, 1.
8 K.-S. Lee, I.-S. Park, Y.-H. Cho, D.-S. Jung, N. Jung, H.-Y. Park and Y.-E. Sung, *J. Catal.*, 2008, **258**, 143.
9 D.-J. Guo and J.-M. You, *J. Power Sources*, 2012, **198**, 127.
10 C. Xu, P. K. Shen and Y. Liu, *J. Power Sources*, 2007, **164**, 527.
11 E. Higuchi, K. Miyata, T. Takase and H. Inoue, *J. Power Sources*, 2011, **196**, 1730.
12 B. Y. Xia, H. B. Wu, J. S. Chen, Z. Wang, X. Wang and X. W. Lou, *Phys. Chem. Chem. Phys.*, 2012, **14**, 473.
13 H. Song, X. Qiu, X. Li, F. Li, W. Zhu and L. Chen, *J. Power Sources*, 2007, **170**, 50.
14 X. Zhang, H. Zhu, Z. Guo, Y. Wei and F. Wang, *J. Power Sources*, 2011, **196**, 3048.
15 R. B. Moghaddam and P. G. Pickup, *Electrochim. Acta*, 2012, **65**, 210.
16 Y. X. Bai, J. J. Wu, J. Y. Xi, J. S. Wang, W. T. Zhu, L. Q. Chen and X. P. Qiu, *Electrochem. Commun.*, 2005, **7**, 1087.
17 H. Song, X. Qiu, F. Li, W. Zhu and L. Chen, *Electrochem. Commun.*, 2007, **9**, 1416.
18 D. A. Konopka, M. Li, K. Artyushkova, N. Marinkovic, K. Sasaki, R. Adzic, T. L. Ward and P. Atanassov, *J. Phys. Chem. C*, 2011, **115**, 3043.
19 L. Jiang, L. Colmenares, Z. Jusys, G. Q. Sun and R. J. Behm, *Electrochim. Acta*, 2007, **53**, 377.
20 L. Jiang, G. Sun, S. Sun, J. Liu, S. Tang, H. Li, B. Zhou and Q. Xin, *Electrochim. Acta*, 2005, **50**, 5384.
21 M. Niederberger, M. H. Bartl and G. D. Stucky, *J. Am. Chem. Soc.*, 2002, **124**, 13642.
22 N. Pinna, G. Neri, M. Antonietti and M. Niederberger, *Angew. Chem., Int. Ed.*, 2004, **43**, 4345.
23 N. Pinna and M. Niederberger, *Angew. Chem., Int. Ed.*, 2008, **47**, 5292.
24 B. Ludi, M. J. Süess, I. A. Werner and M. Niederberger, *Nanoscale*, 2012, **4**, 1982.
25 N. Pinna, *J. Mater. Chem.*, 2007, **17**, 2769.
26 N. Pinna, G. Garnweitner, M. Antonietti and M. Niederberger, *Adv. Mater.*, 2004, **16**, 2196.
27 I. Bilecka, I. Djerdj and M. Niederberger, *Chem. Commun.*, 2008, 886.
28 I. Bilecka and M. Niederberger, *Nanoscale*, 2010, **2**, 1358.
29 I. Bilecka, L. Luo, I. Djerdj, M. D. Rossell, M. Jagodič, Z. Jagličić, Y. Masubuchi, S. Kikkawa and M. Niederberger, *J. Phys. Chem. C*, 2011, **115**, 1484.
30 S. Baek, S.-H. Yu, S.-K. Park, A. Pucci, C. Marichy, D.-C. Lee, Y.-E. Sung, Y. Piao and N. Pinna, *RSC Adv.*, 2011, **1**, 1687.
31 P. A. Russo, N. Donato, S. G. Leonardi, S. Baek, D. E. Conte, G. Neri and N. Pinna, *Angew. Chem., Int. Ed.*, 2012, **51**, 11053.
32 P. J. M. Carrott, R. A. Roberts and K. S. W. Sing, *Carbon*, 1987, **25**, 769.
33 Y.-C. Her, J.-Y. Wu, Y.-R. Lin and S.-Y. Tsai, *Appl. Phys. Lett.*, 2006, **89**, 043115.
34 R. Kou, Y. Shao, D. Mei, Z. Nie, D. Wang, C. Wang, V. V. Viswanathan, S. Park, I. A. Aksay, Y. Lin, Y. Wang and J. Liu, *J. Am. Chem. Soc.*, 2011, **133**, 2541.
35 V. D. Colle, J. Souza-Garcia, G. Tremiliosi-Filho, E. Herrero and J. M. Feliu, *Phys. Chem. Chem. Phys.*, 2011, **13**, 12163.
36 B. Braunchweig, D. Hibbitts, M. Neurock and A. Wieckowski, *Catal. Today*, 2013, **202**, 197.
37 J. L. Margitfalvi, I. Borbáth, M. Hegedűs, Á. Szegedi, K. Lázár, S. Gőbölös and S. Kristyán, *Catal. Today*, 2002, **73**, 343.
38 F. J. Scott, S. Mukerjee and D. E. Ramaker, *J. Phys. Chem. C*, 2010, **114**, 442.